CHAPTER 7

Synthesis of Ni-Zn Ferrite nanopowders by using EDTA based precursor method

7.1 Experimental Procedure for Chemical Synthesis:

The chemicals used were Fe $(NO_3)_3.9H_2O$ (99.9%, Merck, India), Ni $(NO_3)_2.6H_2O$ (99.9%, Merck, India), Zn dust (99.9%, Merck, India), and ethylenediamine tetracetic acid (EDTA, 99.9%, Merck, India) without further purification. $Zn(NO_3)_2$ was prepared by dissolving Zn powder in aqueous nitric acid. EDTA was dissolved in water by adding to it, a 50 percent ammonia solution drop wise till all EDTA was exactly dissolved. The pH of EDTA solution was ~5.

Stoichiometric amounts of metal nitrates were dissolved in distilled water according to the molar compositions as shown in Table 7.1.

Table 7.1. Molar ratio of starting compounds

Target Composition	$Fe(NO_3)_3.9H_2O$	$Ni(NO_3)_2.6H_2O$	Zn powder	EDTA
$Ni_{0.80}Zn_{0.20}Fe_2O_4$	0.084	0.034	0.008	0.126
$Ni_{0.65}Zn_{0.35}Fe_2O_4$	0.084	0.027	0.015	0.126
$Ni_{0.50}Zn_{0.50}Fe_2O_4$	0.084	0.021	0.021	0.126
$Ni_{0.40}Zn_{0.60}Fe_2O_4$	0.084	0.017	0.025	0.126

Aqueous solutions of metal nitrates and EDTA were mixed in a molar ratio of 1:1. The solutions were stirred for 1hour at room temperature using a magnetic stirrer.

Dark brown precursors were formed when the mixtures were evaporated to dryness on a hot plate at ~125^{0}C. The precursor powders were then calcined in air in temperatures ranging from 250 to 450^{0}C for two and a half hours to obtain Ni-Zn ferrite nanopowders [132, 139]. In order to avoid contamination of the precursors by carbon, a few drops of saturated ammonium nitrate solution was added to the precursor powders during calcination.

7.2 Results and Discussion:

7.2.1 Thermal Analysis:

TG-DTG and DSC analyses were performed to investigate the decomposition behavior of the precursor powders due to heat treatment in air and thermograms are shown in Fig 7.1(a-d).

The important features of the thermograms are as follows:

(i) In TG thermogram, a total weight loss of ~ 15-25% (depending on the composition of thr precursor) was observed in the temperature range of 40-550^{0}C.

(ii) Minor weight loss of ~3-5% occurred between 30 and 150^{0}C that can be assigned to the loss of moisture from the samples.

(iii) Major weight loss of ~12-20% occurred in the region from 150 to 550^{0}C and this weight loss was attributed to oxidative decomposition of precursor, accompanied by the evolution of CO_2 and NO_x gases.

(iv) Heating the sample beyond 460^{0}C showed neither a significant weight loss in TG thermogram nor formation of any new peak in DSC thermogram, confirming the completion of decomposition of the precursor to Ni-Zn ferrite phase at ~460^{0}C [132, 139].

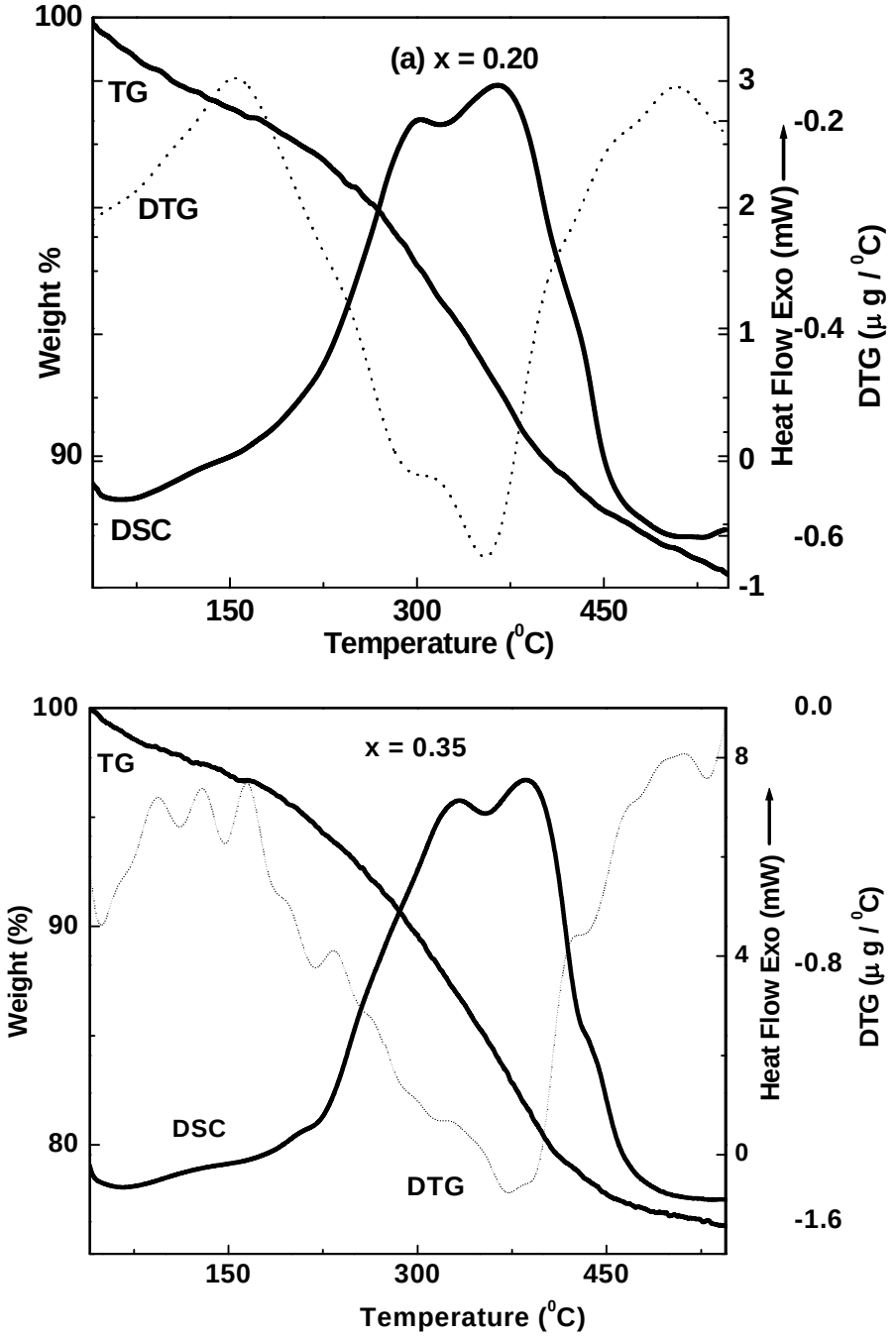

Fig. 7.1 continued

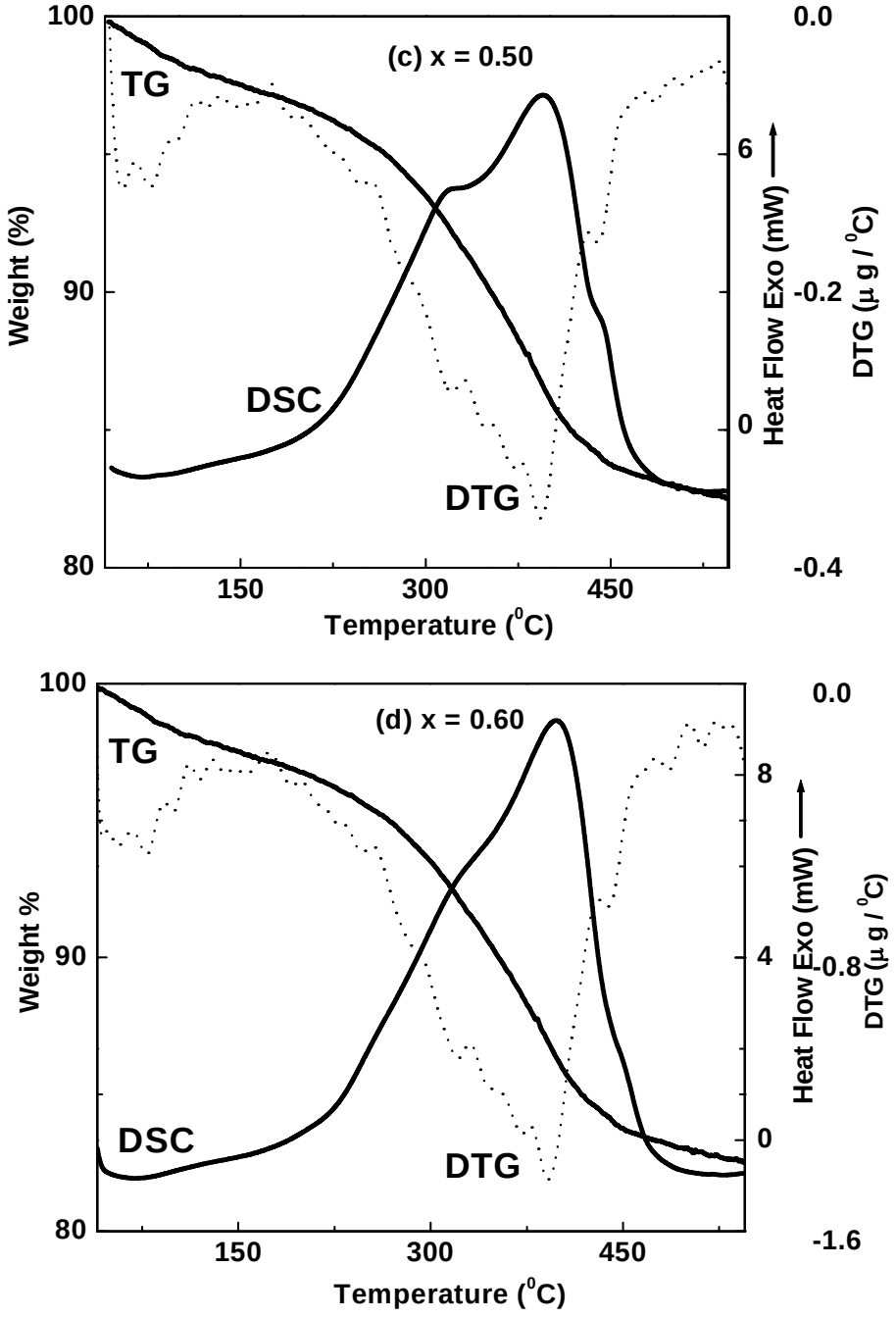

Fig. 7.1 TG-DTG and DSC thermograms of precursor powders for (a) $Ni_{0.80}Zn_{0.20}Fe_2O_4$ (b) $Ni_{0.65}Zn_{0.35}Fe_2O_4$ (c) $Ni_{0.50}Zn_{0.50}Fe_2O_4$ (d) $Ni_{0.40}Zn_{0.60}Fe_2O_4$ in air.

The DSC thermograms of the series of Ni-Zn ferrite precursors were compared and are shown in Fig. 7.2.

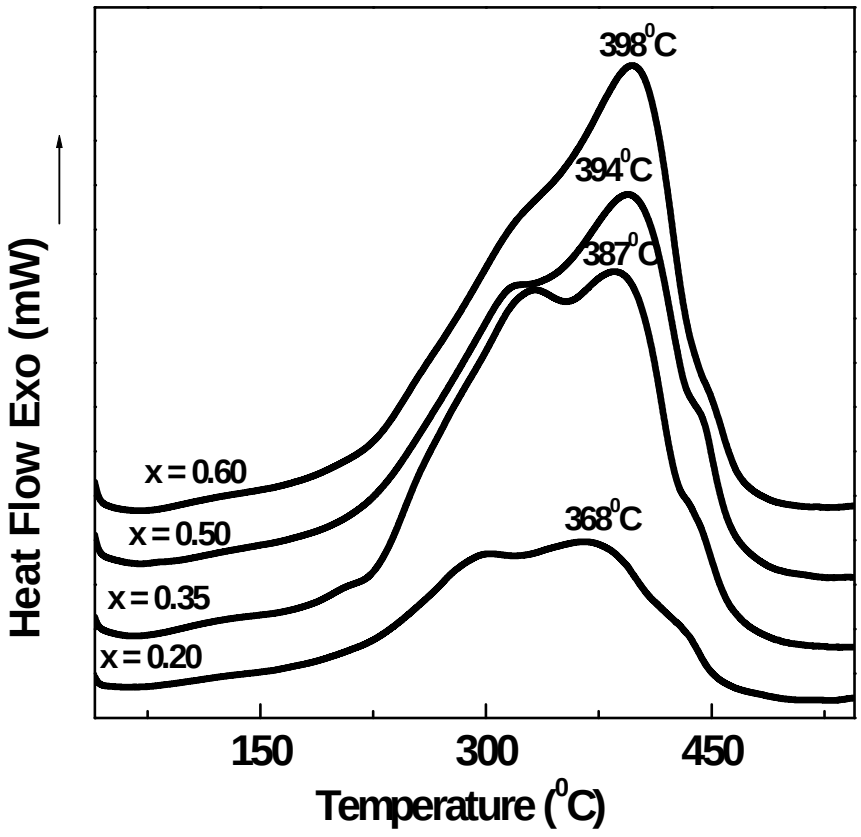

Fig 7.2 DSC thermograms of precursor powders for the series of $Ni_{1-x}Zn_xFe_2O_4$ ferrites.

The exothermic peak corresponding to the oxidative decomposition shifted from 398 to 368^{0}C with increase in Ni^{2+} concentration from (1-x) = 0.40 to 0.80 in the $Ni_{1-x}Zn_xFe_2O_4$ composition. This decrease in decomposition temperature with increase in Ni^{2+} concentration might be due to the catalyzing effect of Ni^{2+} on the decomposition process. The heat liberated (1-3 kJ/g, depending upon the composition) through this process is sufficient for the crystallization of the desired ferrite phase [132, 134, 139].

7.2.2 XRD Analysis:

Room temperature XRD spectra of powders, calcined at different temperatures for all values of x are shown in Fig. 7.3 (a-d).

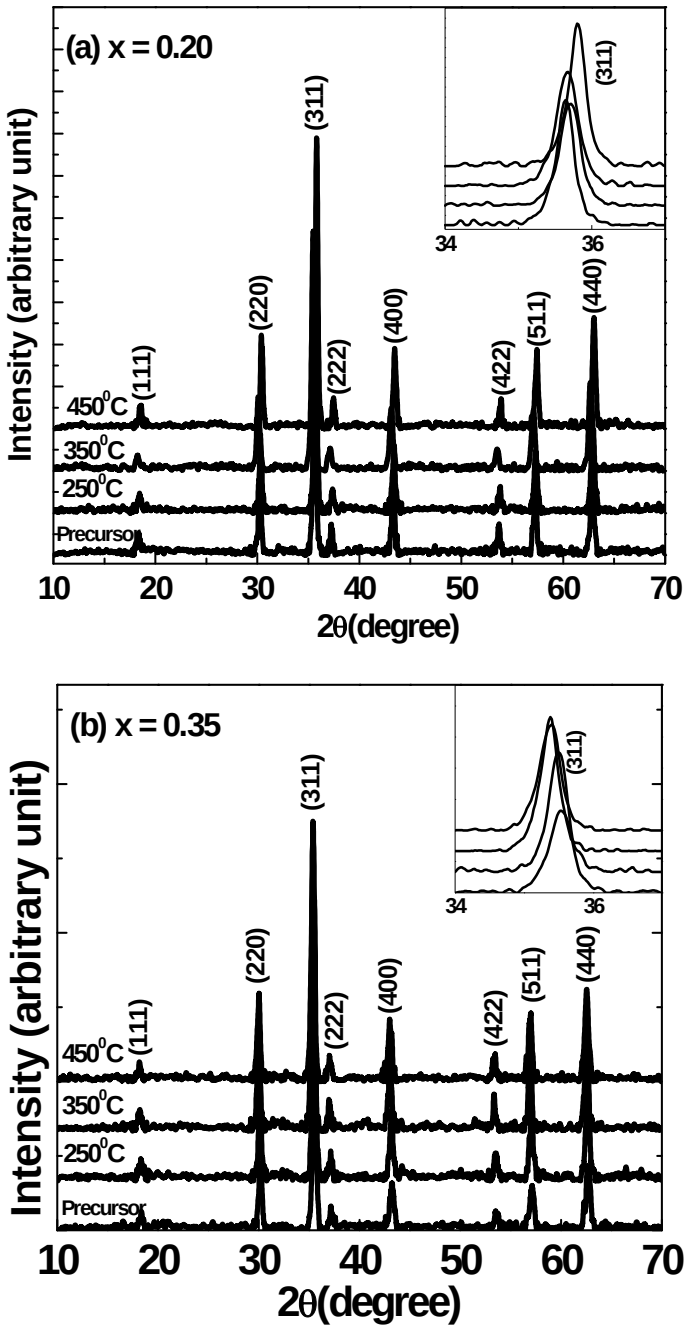

Fig. 7.3 continued

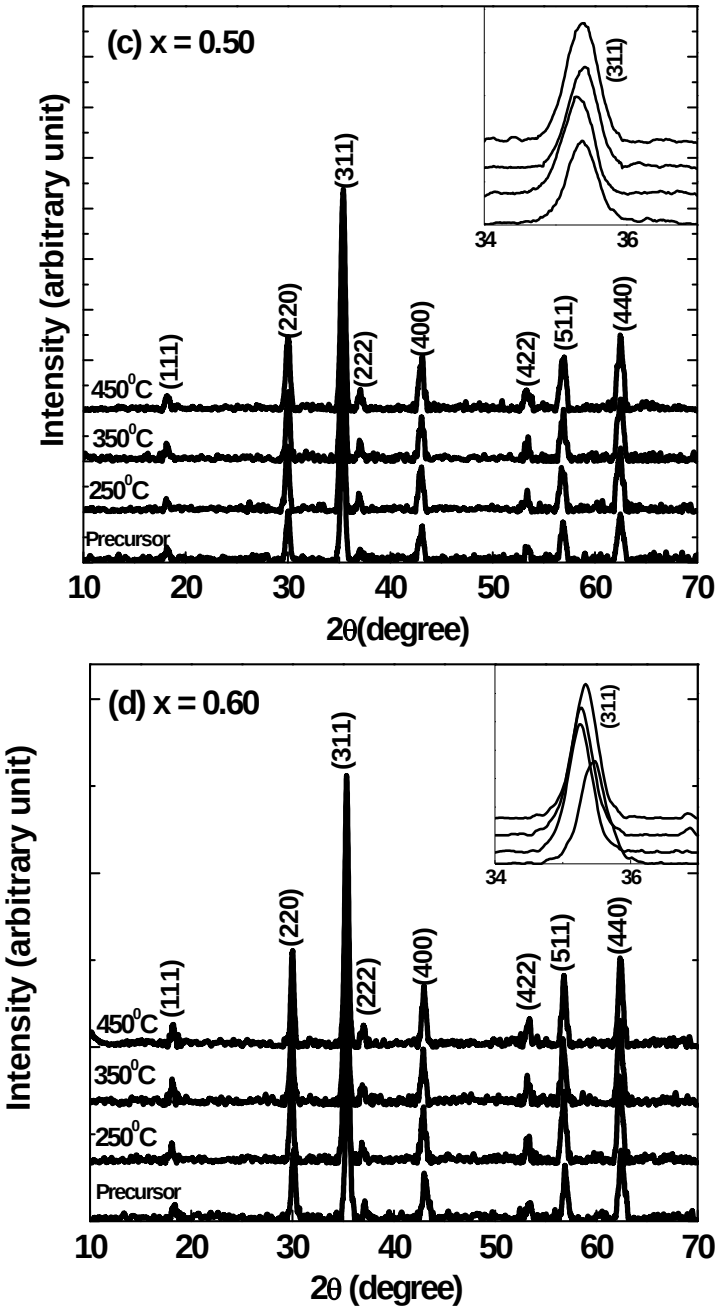

Fig. 7.3 XRD spectra of precursor powders of (a) $Ni_{0.80}Zn_{0.20}Fe_2O_4$ (b) $Ni_{0.65}Zn_{0.35}Fe_2O_4$ (c) $Ni_{0.50}Zn_{0.50}Fe_2O_4$ (d) $Ni_{0.40}Zn_{0.60}Fe_2O_4$ ferrites, at different calcination temperatures. Slow scan of the (311) diffraction plane are shown in the insets.

The main features of the spectra are as follows:

(i) The peaks corresponding to (111), (220), (311), (222), (400), (422), (511) and (440) diffraction planes of Ni-Zn ferrite were present for the precursor (JCPDS 08-0234).

(ii) These peaks were also present for all other calcination temperatures ranging from 250 to 450^0C and correspond to the pure phase of Ni-Zn ferrite [132, 139].

(iii) Impurity phase was not detected during any stage of calcination; there was only an increase in the intensity of the peaks.

(iv) Crystallite size of powders calcined at different temperatures was calculated using Scherrer's [125] equation and they lie in the range of 15-30 nm depending upon the calcination temperature.

7.2.3 TEM Analysis:

TEM micrographs for the powder calcined at 450^0C are shown in Fig. 7.4 (a) and (b). The micrographs clearly indicated that average particle size of the calcined powder was ~35 nm. The particles were mostly spherical in shape and formed loose aggregates.

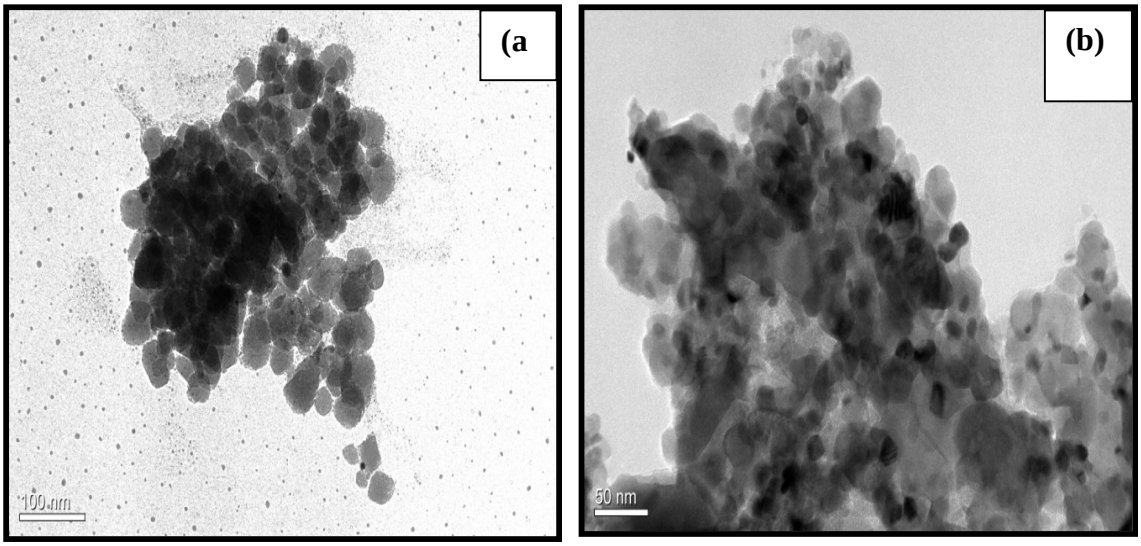

Fig 7.4 TEM micrographs for the series of $Ni_{1-x}Zn_xFe_2O_4$ of nanopowders for (a) x = 0.50 and (b) x = 0.60, synthesized at calcination temperature of 450^0C.

7.2.4 SEM Analysis:

SEM was used to investigate the change of microstructures of the as synthesized $Ni_{1-x}Zn_xFe_2O_4$ nanopowders with change in sintering temperature and composition and these are shown in Fig 7.5 (a-i). For this purpose, four sets of pellets were prepared, (i) one set of pellets was kept unsintered (ii) the other set of pellets were sintered at 1100, 1200 and 1300^0C for 2 hours.

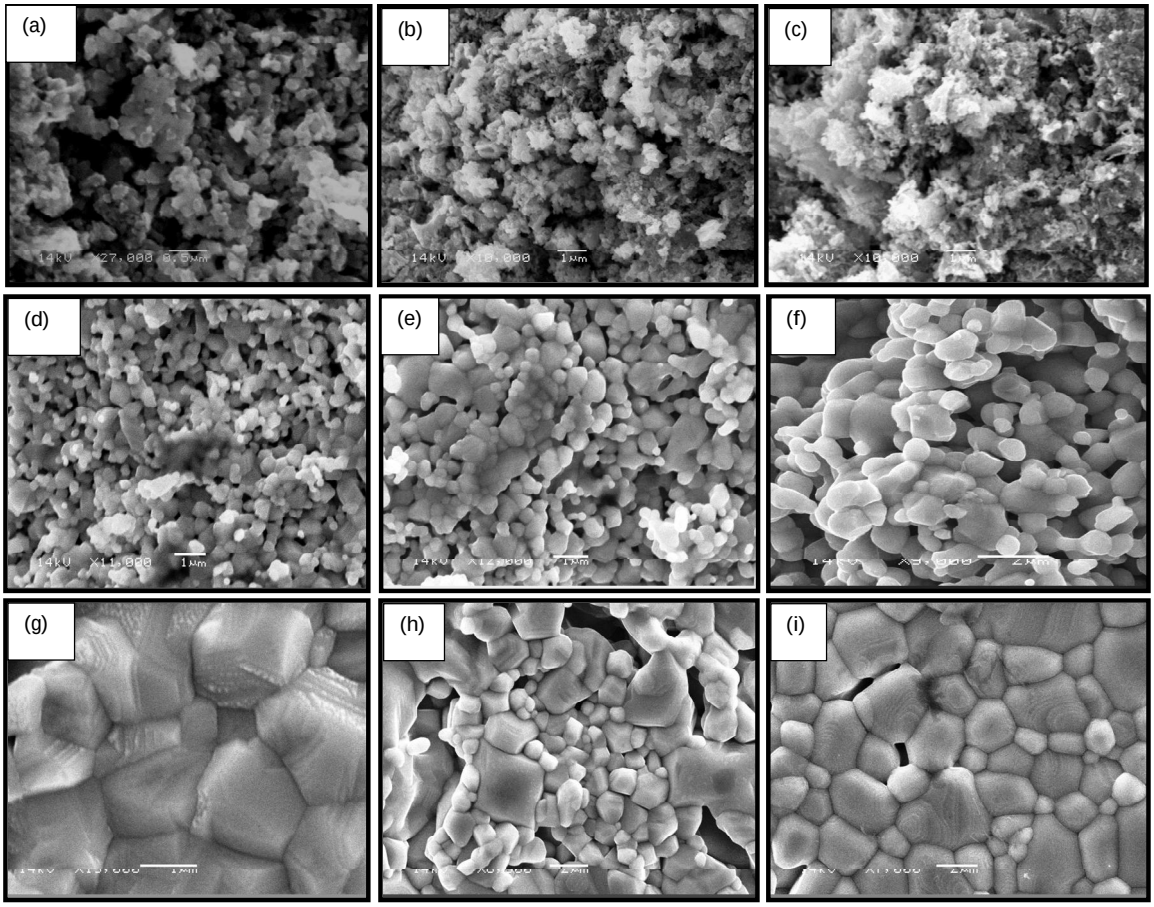

Fig.7.5. SEM micrographs of $Ni_{(1-x)}Zn_xFe_2O_4$ showing the change of microstructure with changing value of x and sintering condition (a) x = 0.20, unsintered, (b) x = 0.35, unsintered, (c) x = 0.60, unsintered, (d) x = 0.35, sintered at 1100^0C, (e) x = 0.50, sintered at 1100^0C, (f) x = 0.20, sintered at 1200^0C, (g) x = 0.60, sintered at 1200^0C, (h) x = 0.20, sintered at 1300^0C, (i) x = 0.60, sintered at 1300^0C.

The main features of SEM micrographs are summarized as follows:

(i) The micrographs of the unsintered samples revealed uniform, agglomerated and spherical shaped nanopowders of Ni-Zn ferrite. (Fig. 7.5(a-c)).

(ii) When sintering temperature was 1100^0C, the grains grew in size and agglomeration was present. The grains for x = 0.50 are larger than the grains for the composition where x = 0.35 (Fig. 7.5(d) and (e)).

(iii) Sintering at 1200^0C resulted in formation of well-defined bigger grain sizes but average grain size was still less than 3μm. The effect of zinc on densification and grain growth at this sintering temperature can clearly be seen by comparing the SEM micrographs (Fig. 7.5(f) and (g)).

(iv) Though sintering temperature was reasonably high (1200^0C), Zn loss was not observed in our samples which ensures the maintenance of stoichiometry of the final product. Inhomogeneity or partial precipitation of impurity phase was not observed for our samples whereas in most of the reported results, Zn loss at high temperatures has been observed in SEM micrographs as pore formation within the grains [66-68].

(v) When sintered at 1300^0C, formation of bigger grains occurred but their grain size distribution became non-uniform, particularly when concentration of Zn is high. There was preferential grain growth as can be seen in Fig. 7.5 (h,i).

7.2.5 DC Resistivity:

DC resistivity of the unsintered and sintered pellets was measured from room temperature (25^0C) to 225^0C by using the two-probe method for all values of x and its variation with temperature is shown in Fig. 7.6. Room temperature resistivity values for the series of composition ($Ni_{1-x}Zn_xFe_2O_4$ with x = 0.20, 0.35, 0.50 and 0.60) sintered at various temperatures are listed in Table 7.2.

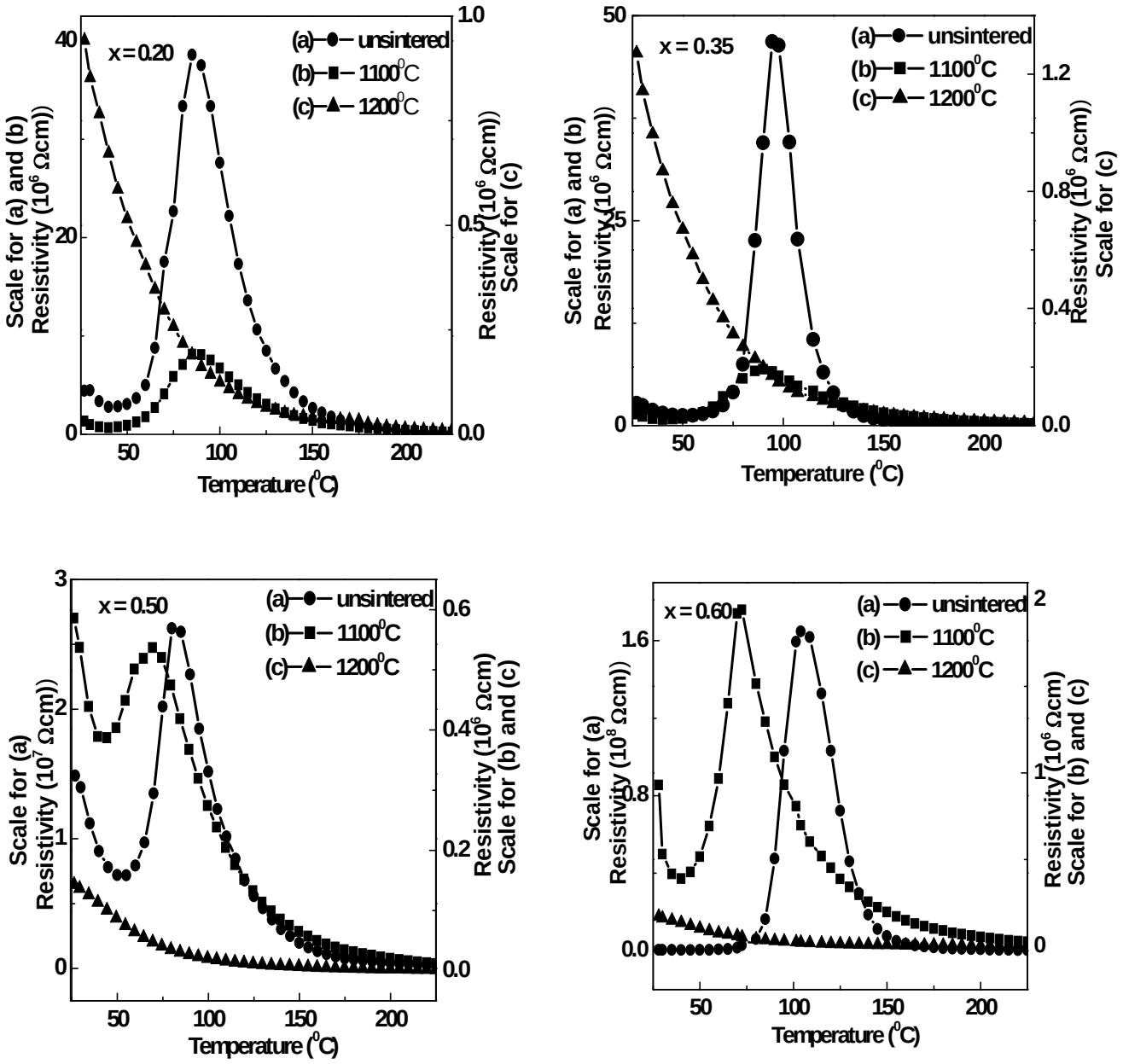

Fig 7.6 DC resistivity for the series of $Ni_{1-x}Zn_xFe_2O_4$ nanopowders with respect to temperature for unsintered samples and samples sintered at 1100 and 1200^{0}C.

Table 7.2. Room temperature (25^0C) DC resistivity of Ni-Zn ferrites for unsintered samples and samples sintered at 1100 and 1200^0C.

Composition $Ni_{1-x}Zn_xFe_2O_4$	DC Resistivity (Ω cm)		
	unsintered	1100^0C	1200^0C
x = 0.20	4.4×10^6	1.3×10^6	0.9×10^6
x = 0.35	2.7×10^6	1.3×10^6	1.3×10^6
x = 0.50	1.5×10^7	5.9×10^5	1.4×10^5
x = 0.60	4.4×10^5	9.3×10^5	1.7×10^5

The impact of microstructure, sintering temperature and composition in the series of $Ni_{1-x}Zn_xFe_2O_4$ ($0 \leq x \leq 1$) powders on the resistivity is discussed below.

(i) Impact of microstructure:

It was observed that the room temperature resistivity of the unsintered samples was of the order of ~10^5-10^7Ωcm depending upon the composition of the nanopowders. With increase in temperature, the resistivity increased and a maximum was recorded in the temperature range of ~ 80-100^0C. This behavior might be attributed to the presence of open porosity, loose agglomeration of ultrafine powders and entrapped moisture inside the pores of the powders (humidity recorded in our lab was ~91% at room temperature) [12, 13, 131, 132, 135, 139]. Increasing the temperature upto ~100^0C caused the evaporation of moisture from the samples and therefore, maximum resistivity (~10^7-10^8 Ωcm) was attained. This maximum in resistivity

corresponds to desorption of moisture from the samples. Beyond ~100^0C, the samples exhibit typical negative temperature coefficient of resistance (NTCR) behavior of ferrites [38]. Such high resistivity can be explained by simply understanding the fact that smaller grains would offer greater resistance to electron path.

When the samples were sintered at 1100^0C, the grains grew in size and also the porosity was reduced. Therefore, the impact of adsorption of moisture in these samples was also less pronounced. Here, the resistivity seem to be affected by the zinc content in the samples especially when x = 0.60.The microstructures of samples sintered at 1200^0C revealed the absence of any intragranular porosity especially for higher Zn concentration (x = 0.60). Therefore, these samples exhibited typical NTCR behavior of ferrites from room temperature to 225^0C.

(ii) Impact of sintering temperature:

Increasing the sintering temperature of the samples from 1100 to 1200^0C resulted in decrease in room temperature resistivities for all the compositions. The reduction in resistivity on increasing the sintering temperature can be attributed to bigger grain sizes with lesser number of insulating grain boundaries, higher amount of densification and absence of porosity in the samples.

(iii) Impact of Zn composition in the series of $Ni_{1-x}Zn_xFe_2O_4$ ($0 < x < 1$) powders:

Zinc is known to promote densification and grain growth in the samples and large grains with lesser number of grain boundaries would cause a decrease in the resistivity [66]. With increasing amount of Zn, a decrease in room temperature resistivity for nanopowders as well as micron sized powders was observed. This, therefore, could be due to increased amount of zinc.

7.2.6 Magnetization Measurement:

Room temperature saturation magnetization (M_s) and coercivity (H_c) of the as-synthesized nanopowders was measured and the hysteresis loops for all compositions are shown in Fig. 7.7. The measured values for the series of composition $Ni_{1-x}Zn_xFe_2O_4$ ($0 < x < 1$) are listed in Table 7.3.

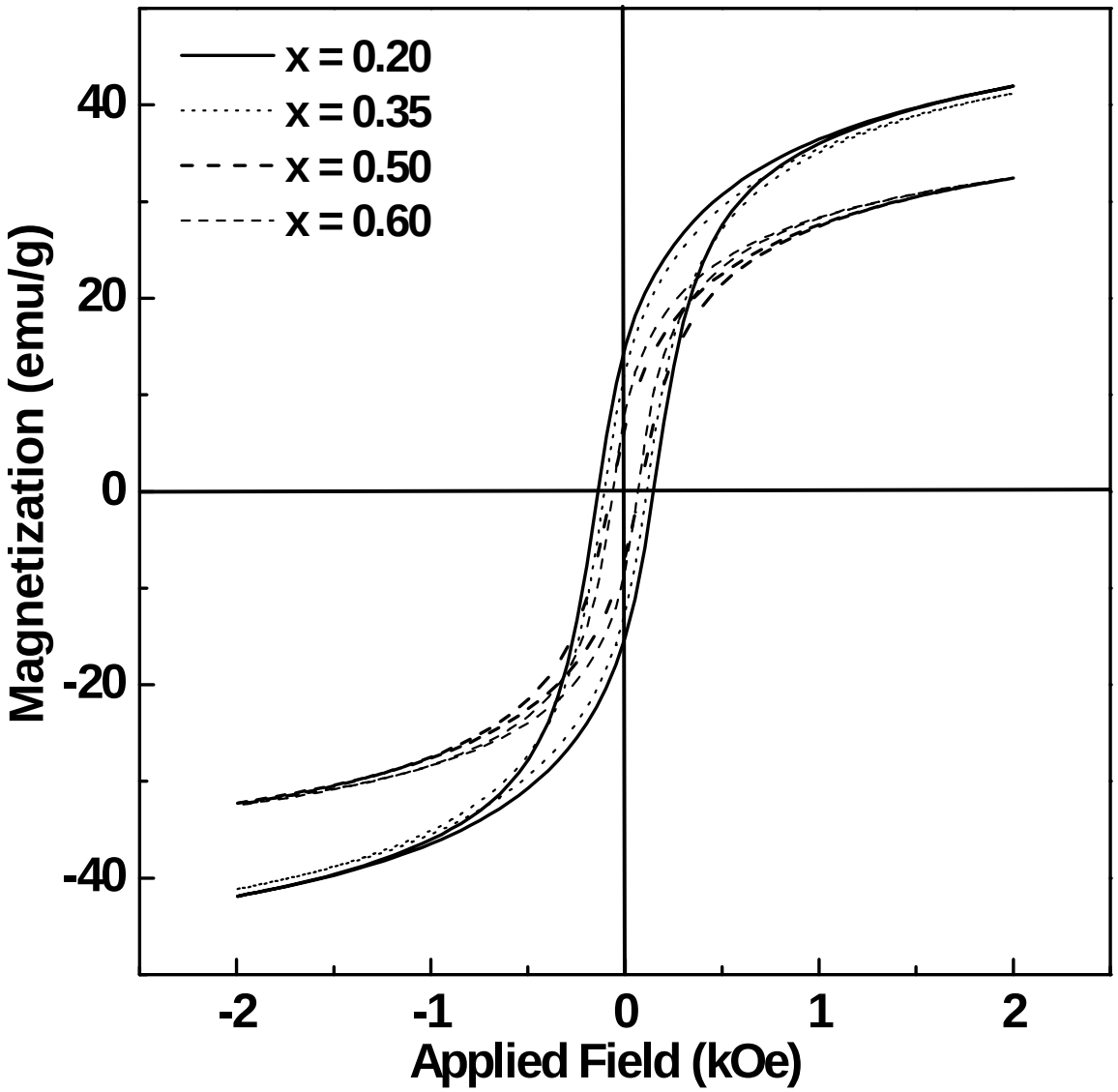

Fig 7.7 Room temperature hysteresis loops for the series $Ni_{1-x}Zn_xFe_2O_4$ nanopowders.

Table 7.3. Room temperature saturation magnetization and coercivity of different compositions.

$Ni_{1-x}Zn_xFe_2O_4$	M_s (emu/g)	H_c (Oe)
x = 0.20	41.9	132
x = 0.35	41.2	103.5
x = 0.50	32.4	64.6
x = 0.60	32.4	65

It was observed that, the saturation magnetization decreased with increasing Zn^{2+} concentration (x= 0.20 - 0.60) from 41.9 to 32.4 emu/g. Zn^{2+} ions have an affinity to occupy tetrahedral (A) sites and Ni^{2+} ions have a tendency to go into the octahedral (B) sites in the crystal lattice, [44] while Fe^{3+} ions are distributed over both the sites. It might happen that as the concentration of diamagnetic Zn^{2+} on A sites is increased, the Fe^{3+} ions were pushed from A to B sites. This decrease in the magnetic ions at A site resulted in a weakened A-B exchange coupling and hence a diminished moment [43].

Discussion

TGA-DSC, XRD and TEM analysis of the synthesized precursors and calcined powders confirmed that oxidative decomposition of precursor lead to the formation of single phase Ni-Zn ferrite nanopowders. In this chemical method, a homogeneous aqueous solution of metal nitrates and EDTA, on complete dehydration, produces a fluffy, voluminous, carbon-rich mass known as “precursor” powder.

The chelating agent, EDTA, plays a critical role. It not only prevents the segregation or intermittent precipitation of metal ions from solution during evaporation but also acts as the fuel to provide the heat through combustion for the formation of the metal oxide phase. During thermal decomposition of precursor, nascent metal oxides forms, which are small atomic clusters with proper chemical homogeneity and these nascent metal oxides finally produce Ni-Zn ferrite nanopowders. The heat provided by the carbonaceous mass of the precursor during thermal decomposition helps in lowering down of the external temperature required for the formation of the phase. Moreover, the evolution of various gases (such as water vapour, CO, CO_2, NO_x) during decomposition of the precursor helps it to disintegrate and dissipate the heat of decomposition. This inhibited the sintering of fine particles during the process to produce nanosized Ni-Zn ferrite [57, 123].

DC resistivity measurements indicated that it was strongly correlated with the sintering condition and the composition and hence the microstructure of the samples. The resistivity of the nanopowders was found to be affected by moisture due to their high porosity and low green density (~2.5 g/cm^3). However, for the samples sintered at 1100^{0}C, the effect of moisture is less pronounced as sintering results in densification (sintered density~2.8-3.2 g/cm^3) and grain growth. For the samples sintered at an even higher temperature of 1200^{0}C, the effect of moisture is absent (sintered density ~3.4-4.2 g/cm^3) and the samples exhibited the typical NTCR behavior of ferrites.

7.4 Summary of Results:

1. Ni-Zn ferrite nanopowders were successfully synthesized by using EDTA precursor based synthesis method.
2. Major thermal decomposition of the precursor was complete at ~460^{0}C.
3. Single phase Ni-Zn ferrite was formed at a calcination temperature of 450^{0}C for two and a half hours in air atmosphere.
4. Average particle size of the nanopowders was ~ 35 nm.
5. Surface morphology studies revealed that the nanoparticles were round in shape.
6. Room temperature resistivity of as-synthesized nanopowder was in the range ~10^5 - 10^7 Ω cm.

7. Room temperature saturation magnetization varied in the range of 32.4 to 41.9 emu/g and the coercivity varied between 65 and 132 Oe depending on the composition.